Soliton Mode-Locking with Saturable Absorbers

F. X. Kärtner, I. D. Jung, and U. Keller

(Invited Paper)

***Abstract*— We investigate ultrashort pulse generation based on the fundamental soliton generation that is stabilized by a saturable absorber. The case of an absorber with a recovery time much longer than the pulsewidth of the generated soliton is investigated in detail. Based on soliton perturbation theory we derive equations for the soliton variables and the continuum generated in a mode-locked laser. Analytic criteria for the transition from stable to unstable soliton generation are derived. The results demonstrate the possibility of ultrashort pulse generation by a slow saturable absorber only. The theoretical results are compared with experiments. We generate pulses as short as 13 fs using only semiconductor saturable absorbers.**

I. Introduction

OVER the last years great progress in the production of femtosecond pulses has been achieved. Colliding pulse mode-locked lasers, producing pulses as short as 27 fs were replaced by the Kerr-lens-mode-locked (KLM) Ti:sapphire lasers [2]–[4]. This new solid state laser material together with KLM allows for a routine production of 10-fs pulses and lower [5]–[8], if the higher order dispersion is carefully controlled [9], [10]. Due to the nonresonant nature of the Kerr effect in crystals, KLM can be used to mode-lock lasers from the visible to the near infrared without any additional intracavity elements. Despite its success, KLM has also some disadvantages. KLM is based on the generation of an artificial fast saturable absorber effect due to the self-focusing that occurs inside the laser crystal [11] for subpicosecond pulses. To enhance self-focusing one usually operates the cavity close to the stability limit, so that the cavity is sensitive to small additional intracavity lensing effects [11], [12]. Thus, KLM interrelates the laser modes with the laser dynamics. This leads to a complex spatio-temporal laser dynamics [13] and results in a restricted cavity design. Furthermore, very short pulse lasers based on a fast saturable absorber alone, have an intrinsic problem to self-start from a continuous-wave (CW)-operation. This is simply due to the fact, that the peak intensity changes by about six orders of magnitude when the laser switches from CW-operation, where the pulse energy is distributed over about 10 ns, to a 10-fs pulse. Thus, nonlinear effects which are in the order of one in pulsed operation are of the order of 10^{-6} in CW-operation, if the absorber is not completely oversaturated when it reaches steady-state pulsing. Currently, self-starting KLM lasers have been demonstrated down to about 50 fs [14], [15] in cavities optimized for self-starting. Even then, the measured mode-locking build-up time is in the order of several milliseconds. Thus, usually separate starting mechanisms are required [4], [16].

In order to generate the shortest pulses, the modulation depth of the absorber has to be maximum. In a KLM laser the generated artificial, saturable absorption and the self-phase modulation have the same origin: the intensity dependent refractive index. Recent measurements of the beam waist in KLM lasers suggest, that the self-phase modulation (SPM) in sub-10-fs lasers is overdriven and might limit further pulse shortening.

Recently, we have shown theoretically, that femtosecond solid-state lasers can generate ultrashort solitonlike pulses when mode-locked only by a slow saturable absorber. By a slow saturable absorber we understand an absorber with a recovery time much longer than the final pulsewidth [18]. This is a regime of mode-locking, where the pulse is completely shaped by soliton formation, i.e., the interplay between negative group-delay dispersion (GDD) and SPM. The absorber dynamics only stabilizes the soliton against the growth of background radiation. In the final stage of pulse formation, it is the solitonlike pulse shaping that locks the modes together. With this method we can generate pulses, which are considerably shorter than the recovery time of the absorber. Therefore, we call this scheme soliton mode-locking stabilized by a slow saturable absorber.

It is well known that solitonlike pulse shaping, due to SPM and GDD generates pulses that are both shorter and more stable [5], [9], [19], [20]. Both mechanisms are the ingredients for the existence of average, or guiding center solitons [21] in mode-locked lasers. These solitons are governed by a perturbed nonlinear Schrödinger equation [22] as long as the changes of the pulse in the nonlinear elements per round-trip are small [23], [24]. However, the traditional mode-locking schemes [25] rely either on a fast saturable absorber, as is the case for additive-pulse or KLM mode-locked systems [20], [26], [see Fig. 1(a)] or on the interplay between a slow saturable absorber and gain saturation, as is the case with dye lasers [27], [28], [see Fig. 1(b)]. The two mechanisms open a net gain window in time so that only the pulse itself experiences gain per round-trip. This permits the system to discriminate against noise that may grow outside the net gain window, and therefore the pulse is kept stable against perturbations or noise.

In contrast to these well-known schemes, in a soliton mode-locked laser stabilized by a slow absorber the net gain window

Manuscript received September 11, 1996; revised January 10, 1997. This paper was supported by the Swiss National Science Foundation.

The authors are with the Swiss Federal Institute of Technology, Institute of Quantum Electronics, Ultrafast Laser Physics Laboratory, ETH Hönggerberg HPT, CH-8093 Zürich.

Publisher Item Identifier S 1077-260X(96)09678-5.

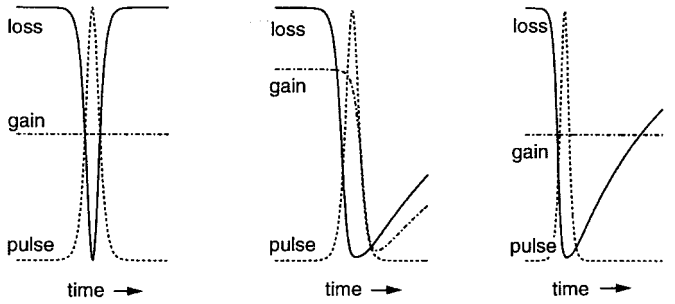

Fig. 1. Pulse-shaping and stabilization mechanisms owing to gain and loss dynamics in a mode-locked laser in case of using: (a) a fast saturable absorber, (b) a slow saturable absorber plus slow gain saturation, and (c) a slow saturable absorber plus soliton formation.

does not close immediately after passage of the pulse, [see Fig. 1(c)]. This is possible in the soliton regime because, for the soliton, the nonlinear effects due to SPM and the linear effects owing to the negative GDD are in balance. In contrast, the noise or instabilities that would like to grow are not intense enough to experience the nonlinearity and are therefore spread in time. However, when they are spread in time they are even absorbed by a slowly recovering absorber. Then, the instabilities experience less gain per round-trip than the soliton and they decay with time. We verified this theoretical prediction experimentally, by showing that a semiconductor saturable absorber with a 10-ps response can generate pulses as short as about 300 fs [29]. Meanwhile, based on this principle, we can generate pulses as short as 13 fs by using broadband semiconductor saturable absorbers [30]. This is clearly a regime which was previously only possible by KLM. But in addition to KLM-lasers our pulses are self-starting with mode-locking build-up times in the 200-μs regime. Since, we use real absorbers we can independently optimize the self-phase modulation and the saturable absorption so that the laser self-starts reliably without overdriving the SPM when reaching steady-state pulsed operation. The use of real absorbers also has drawbacks: the absorber can be damaged due to the deposited heat and the absorber has to be designed for a broad bandwidth if short pulses have to be achieved. However, as will be demonstrated by the experimental results, this is manageable.

The paper is organized as follows. First we set the theoretical treatment presented in [18] on a firm foundation and also include refractive index changes due to the absorber, which seem to become very important when using semiconductor absorbers. Then, we use soliton perturbation theory to derive stability relations against the growth of background radiation. Based on these relations, we derive limits with respect to pulsewidth that can be achieved with a given absorber. In Section V, we compare the theoretical results with experiments and show that self-starting lasers in the 10-fs range can be constructed using only semiconductor saturable absorbers and soliton mode-locking. In Section VI, we perform numerical simulations, which demonstrate that the experimental results so far achieved can be understood within the theoretical models discussed in this paper.

II. Basic Model of Soliton Modelocking With Saturable Absorbers

In this section, we set up the basic model for a laser mode-locked with a saturable absorber and derive the governing equations that describe the mode-locking process. The laser pulse that builds up in the cavity will experience changes over one round-trip due to GDD, SPM, gain, loss, filter action due to the finite gain, output coupler and mirror bandwidth, a time dependent absorption and phase change due to the absorber (see Fig. 2). Following the master equation approach of Haus [31], we obtain for the equation of motion of the laser pulse averaged over one round-trip

$$T_R \frac{\partial A(T,t)}{\partial T} = -iD\frac{\partial^2 A}{\partial t^2} + i\delta|A|^2 A + \left[g - l + D_{g,f}\frac{\partial^2}{\partial t^2} - q(T,t)\right]A(T,t). \quad (1)$$

Here, $A(T,t)$ is the slowly varying field envelope, T_R the cavity round-trip time, D the intracavity GDD, $D_{g,f} = g/\Omega_g^2 + 1/\Omega_f^2$ the gain and intracavity filter dispersion. Ω_g and Ω_f are the HWHM gain and filter bandwidth, respectively. The SPM-coefficient δ is given by $\delta = (2\pi/\lambda_0 A_L)n_2\ell_L$, where n_2 is the intensity dependent refractive index of the laser crystal, λ_0 the center wavelength of the pulse and A_L and ℓ_L the effective mode area in the laser crystal and length of the light path through the laser crystal within one round-trip, respectively. The frequency independent losses per round-trip are denoted by l, $g = g_0/[1 + W/(P_L T_R)]$ is the saturated gain, g_0 the small signal gain, and P_L the saturation power. W is the pulse energy

$$W = \int_{-T_R/2}^{T_R/2} |A(T,t)|^2\, dt. \quad (2)$$

We assume a gain medium with a long relaxation time and a large saturation energy. Therefore, the gain is only appreciably saturated by a series of successive pulses traveling through the gain medium, i.e., we neglect the gain saturation during each individual pulse. $q(T,t)$ is the response of the saturable absorber due to an ultrashort pulse. We assume that the pulse is much longer than the transverse relaxation time of the absorber, i.e., the absorber is broad band, so that we can neglect coherent effects in the absorber. Then the absorber dynamics is described by the simple rate equation

$$\frac{\partial q(T,t)}{\partial t} = -\frac{q - q_0}{\tau_A} - \frac{|A(T,t)|^2}{E_A}\, q. \quad (3)$$

Here, τ_A denotes the relaxation time and E_A the saturation energy of the absorber. If the absorber is a two level absorber, driven at resonance, with a transverse relaxation time much shorter than the pulsewidth, the associated change in the refractive index can be neglected. However, in the case of semiconductor absorbers the free carriers generated in the material contribute to the refractive index. Because the saturation of the absorption and the refractive index change are related to the excited carrier density, we assume that they

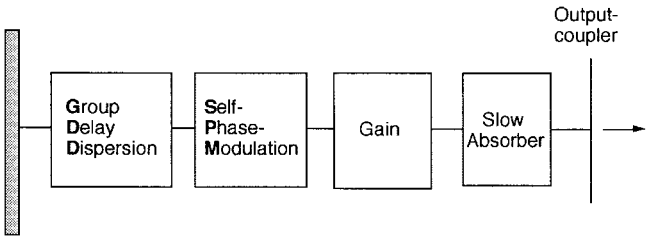

Fig. 2. Schematic of the laser model described by the master equation of mode-locking.

are proportional to each other like in semiconductor lasers. The refractive index change is then implemented in the master equation (1) by a complex saturable absorption

$$q(T, t) \rightarrow q(T, t)(1 + i\alpha) \tag{4}$$

where the α-parameter, often called the linewidth enhancement factor, is the ratio between the amplitude absorption and the refractive index changes [33]. Note, that the α-parameter used here is twice the value usually used in literature since (1) describes the dynamics of the field amplitude and not of the field intensity.

The basic equation (1) is a generalized Ginzburg–Landau equation describing an enormous wealth of physical phenomena in nonequilibrium phase transitions in general [32] and fluid flow [34], [35] in particular. No analytic solutions to the full master (1) are known. Without the dissipative terms due to gain and loss, (1) reduces to the nonlinear Schrödinger equation that has the following fundamental soliton solution in case of negative GDD [22]

$$A_s(T, t) = A_0 \operatorname{sech}[x(T, t)] e^{i\theta(T, t)} \tag{5}$$

where

$$x = \frac{1}{\tau}(t + 2Dp_0T - t_0) \tag{6}$$

is a retarded time normalized to the soliton width τ. The total phase is given by

$$\theta = -p_0 t - D\left(\frac{1}{\tau^2} - p_0^2\right)\frac{T}{T_R} + \theta_0. \tag{7}$$

Yet, the collective variables of the soliton, i.e., its amplitude, phase, center frequency, and timing shift are not fixed. Therefore, we have introduced in addition, a frequency offset p_0 from the assumed carrier frequency, a timing shift t_0 and a initial phase θ_0. The energy contained in the soliton is related with its amplitude via

$$\begin{aligned} W &= \int_{-\infty}^{\infty} |A_s(T, t)|^2 \, dt \\ &= 2A_0^2\tau. \end{aligned} \tag{8}$$

The FWHM of the soliton is given by $\tau_{\mathrm{FWHM}} = 1.76\tau$. The soliton is a consequence of the balance between GDD and SPM. This balance is achieved when the chirp introduced by GDD is compensated by the nonlinear phase shift due to SPM that leads to

$$\begin{aligned} \Phi_0 &= \frac{|D|}{\tau^2} \\ &= \frac{1}{2}\delta A_0^2 \\ &= \frac{\delta W}{4\tau}. \end{aligned} \tag{9}$$

To find an approximate solution of the master equation (1) we will later use soliton perturbation theory.

III. Absorber Response

It is instructive for the following sections, to solve the saturable absorber equation for a sech-shaped pulse

$$A_s(t) = A_0 \operatorname{sech}\left(\frac{t}{\tau}\right), \tag{10}$$

and a sech-shaped pulse with a small perturbation ΔA

$$A_{sp}(t) = A_0 \operatorname{sech}\left(\frac{t}{\tau}\right) + \Delta A\left(\frac{t}{\tau}\right). \tag{11}$$

Introducing the normalized time $x = t/\tau$ (3) reads with (11) up to the first order in the perturbation

$$\begin{aligned} \frac{\partial q(x)}{\partial x} = &-\epsilon(q - q_0) \\ &- \frac{y}{2} q\left[\operatorname{sech}^2(x) + \frac{\Delta A + \Delta A^*}{A_0}\operatorname{sech}(x)\right]. \end{aligned} \tag{12}$$

Here, $\epsilon = \tau/\tau_A$ is the ratio between the pulsewidth and the absorber recovery time and $y = W/E_A$ is the ratio between the pulse energy and the saturation energy of the absorber. This differential equation is linear in q and, therefore, its solution up to first order in the perturbation is given by

$$\begin{aligned} q(x) = q_s(x) &- \int_{-\infty}^{x} dx'' \\ &\cdot \exp\left\{-\epsilon(x - x'') - \frac{y}{2}[\tanh(x) - \tanh(x'')]\right\} \\ &\times \left[\frac{\Delta A(x'') + \Delta A^*(x'')}{A_0}\frac{y}{2} q_s(x'')\operatorname{sech}(x'')\right] dx'' \end{aligned} \tag{13}$$

where q_s is the solution to the sech-shaped pulse only

$$\begin{aligned} q_s(x) = q_0\epsilon \int_{-\infty}^{x} \exp &\left\{-\epsilon(x - x')\right. \\ &\left. -\frac{y}{2}[\tanh(x) - \tanh(x')]\right\} dx'. \end{aligned} \tag{14}$$

In the case of an infinitely slow absorber, i.e., $\epsilon = 0$, the unperturbed absorption is explicitly given by

$$q_{s,\epsilon=0}(x) = q_0 \exp\left\{-\frac{y}{2}[1 + \tanh(x)]\right\}. \tag{15}$$

For the case of a fast absorber, $\epsilon \rightarrow \infty$, we obtain

$$q_{s,\epsilon\rightarrow\infty}(x) = \frac{q_0}{1 + \dfrac{|A|^2}{P_A}}, \qquad \text{where} \quad P_A = \frac{E_A}{\tau_A} \tag{16}$$

is the saturation power of the absorber. Fig. 3 shows the pulse and the unperturbed absorber response for different values of

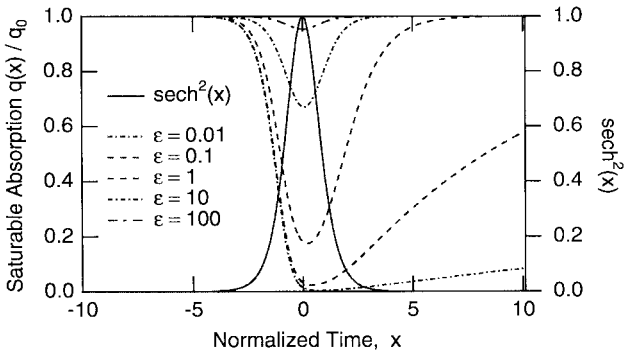

Fig. 3. Response of a saturable absorber for different ratios between pulsewidth and absorber recovery time ϵ. Fast absorber limit $\epsilon = \infty$, slow absorber limit $\epsilon = 0$.

the normalized absorber recovery time but a fixed pulse energy five times the saturation energy of the absorber, $y = 5$. In the case of a nonsaturated absorber the pulse and the change in absorption overlap completely. If the absorber is also fast, the absorption change is a picture of the pulse shape itself and therefore becomes symmetric. A fast absorber also saturates with the pulse intensity rather than with the pulse energy. In contrast, a slow absorber saturates with the pulse energy and shows a strong asymmetric response. Thus only the front wing of the pulse experiences absorption. If the absorber is strongly saturated, $y \gg 1$ and in the case of a slow absorber or $y/\epsilon \gg 1$, the absorption change and the pulse do not overlap any more. This is important, because then the response of the absorber onto a perturbed pulse, [see (12) and (13)], no matter whether the absorber is fast or slow, goes to the first order independent of the perturbation. This means, that the absorber response mostly depends on the pulse energy and not on the detailed shape in contrast to an unsaturated fast saturable absorber. Later, we will focus on the case of strongly saturated absorbers. For a pulse much shorter than the recovery time of the absorber the response of the absorber is essentially independent of the pulse shape and is roughly given by $q_s(t) = q_0 - \hat{q}\exp[-t/\tau_A]$ for $t > 0$ assuming the pulse arrives at $t = 0$. The depth of the modulation is given by

$$\hat{q} = q_0\left(1 - \exp\left[-\frac{W}{E_A}\right]\right) \tag{17}$$

and depends only on the pulse energy and the saturation energy E_A.

IV. Soliton Dynamics Stabilized by a Saturable Absorber

Application of soliton perturbation theory to (1) gives equations for the four collective variables of the soliton and the continuum generated by the perturbations on the soliton. We assume that the solution of the full master equation (1) is a soliton with time dependent soliton parameters, amplitude, center frequency, phase and timing plus a small continuum contribution

$$A(T, t) = [a(x)e^{-ipt} + a_c(T, t)]e^{i\theta} \tag{18}$$

with

$$a(x) = A\,\mathrm{sech}\,(x),$$

and

$$x = \frac{1}{\tau}\left[t + 2D\int_0^T p(T')\,dT' - t_0\right] \tag{19}$$

where a_c is the continuum contribution. The phase is determined by

$$\theta(T) = \theta_0(T) - \frac{D}{T_R}\int_0^T \left[\frac{1}{\tau(T')^2} - p(T')^2\right] dT' \tag{20}$$

whereby we always assume that the relation between the soliton energy and soliton width is maintained

$$\frac{|D|}{\tau(T)^2} = \frac{\delta A(T)^2}{2}. \tag{21}$$

Application of soliton perturbation theory using the notation developed in [38] gives the following set of coupled differential equations for the soliton parameters and the continuum generated:

$$T_R\frac{\partial W}{\partial T} = 2\left[g - l - \frac{D_{g,f}}{3\tau^2} - D_{g,f}p^2 - \tilde{q}_s(W)\right]W + \langle \mathbf{f}_w^{(+)}|(\mathbf{R} + \mathbf{R_D})\mathbf{a}_c\rangle \tag{22}$$

$$T_R\frac{\partial p}{\partial T} = -\frac{4}{3}\frac{D_{g,f}}{\tau^2}p + \tilde{p}_s(W) + \langle \mathbf{f}_p^{(+)}|(\mathbf{R} + \mathbf{R_D})\mathbf{a}_c\rangle \tag{23}$$

$$T_R\frac{\partial t_0}{\partial T} = \tilde{t}_s(W) + \langle \mathbf{f}_t^{(+)}|(\mathbf{R} + \mathbf{R_D})\mathbf{a}_c\rangle \tag{24}$$

$$T_R\frac{\partial \theta_0}{\partial T} = \tilde{\theta}_s(W) + \frac{\partial p}{\partial T}\left(2\int_0^T Dp\,dT' + T_R t_0\right) + \langle \mathbf{f}_\theta^{(+)}|(\mathbf{R} + \mathbf{R_D})\mathbf{a}_c\rangle. \tag{25}$$

As has been shown in [38] the continuum can be written as

$$\mathbf{a}_c = \int_{-\infty}^{\infty} dk[g(k)|\mathbf{f}_k > + \overline{g}(k)|\overline{\mathbf{f}}_k >] \tag{26}$$

where the spectra of the continuum $g(k)$ and $\overline{g}(k)$ are related by

$$\tilde{g}(k) = g(-k)^*. \tag{27}$$

The continuum is determined by the spectrum through

$$a_c = -\frac{\partial^2 G(x)}{\partial x^2} + 2\tanh(x)\frac{\partial G(x)}{\partial x} - \tanh^2(x)G(x) + G^*(x)\,\mathrm{sech}^2(x) \tag{28}$$

where $G(x)$ is Gordon's associated function [36], which is the inverse Fourier transform of the spectrum

$$G(x) = \int_{-\infty}^{\infty} g(k)e^{ikx}\,dk. \tag{29}$$

Therefore, we obtain for the time evolution of the continuum

$$T_R\frac{\partial g(k)}{\partial T} = -i[\tilde{\Phi}_0 + \Phi_0 k^2 + 2\Phi_0 kp\tau] + \langle \mathbf{f}_k^{(+)}|(\mathbf{R} + \mathbf{R_D})\mathbf{a}_c\rangle + \langle \mathbf{f}_k^{(+)}|\mathbf{R}\mathbf{a}(x)e^{-ipt}\rangle \tag{30}$$

with the redefined phase shift per round-trip

$$\tilde{\Phi}_0 = \Phi_0 + T_R \frac{\partial \theta_0}{\partial T} + \Phi_0 (p\tau)^2 - T_R p \frac{\partial t_s}{\partial T}. \tag{31}$$

Here, we have introduced the following abbreviations. The continuum vector $\mathbf{a}_c$ is given by (a_c, a_c^*) and the soliton vector $\mathbf{a}$ is defined analogously. The operator $\mathbf{R}$ describes the linearized action of gain and loss:

$$\mathbf{R} = g\left(1 + \frac{1}{\Omega_g^2 \tau^2} \frac{\partial^2}{\partial x^2}\right) - l - q_s(t) \begin{pmatrix} 1 + i\alpha & 0 \\ 0 & 1 - i\alpha \end{pmatrix} \tag{32}$$

where $q_s(t)$ is the absorber response when saturated by the soliton. This response is given by the solution of (3) with $A(T, t) = a_s(T, t)$, as discussed in Section III. Note, that the linearization of the absorber response to first order in the continuum, i.e., the perturbation to the soliton, is negligible for a strongly saturated absorber, as discussed at the end of Section III and which we will assume for the following. The vectors $\mathbf{f}_w^{(+)}$, $\mathbf{f}_\theta^{(+)}$, $\mathbf{f}_p^{(+)}$, and $\mathbf{f}_t^{(+)}$ project onto the soliton energy, phase, carrier frequency and timing due to the perturbations added to the soliton dynamics. Analogously, the vectors $\mathbf{f}_k^{(+)}$ project onto the continuum contribution. A detailed definition of the projection functions can be found in [38]. The quantities with a tilde describe the shift in the soliton variables per round-trip due to the response of the saturable absorber excited by the soliton

$$\tilde{q}_s(W) = \frac{1}{W} \left\langle \mathbf{f}_w^{(+)} | q_s(t) a_s(t) \begin{pmatrix} 1 + i\alpha \\ 1 - i\alpha \end{pmatrix} \right\rangle \tag{33}$$

$$\tilde{p}_s(W) = \left\langle \mathbf{f}_p^{(+)} | q_s(t) a_s(t) \begin{pmatrix} 1 + i\alpha \\ 1 - i\alpha \end{pmatrix} \right\rangle \tag{34}$$

$$\tilde{t}_s(W) = \left\langle \mathbf{f}_t^{(+)} | q_s(t) a_s(t) \begin{pmatrix} 1 + i\alpha \\ 1 - i\alpha \end{pmatrix} \right\rangle \tag{35}$$

$$\tilde{\theta}_s(W) = \left\langle \mathbf{f}_\theta^{(+)} | q_s(t) a_s(t) \begin{pmatrix} 1 + i\alpha \\ 1 - i\alpha \end{pmatrix} \right\rangle. \tag{36}$$

The remaining operator $\mathbf{R_D}$ describes the additional dynamics introduced as long as the soliton parameters do not reach their steady-state values

$$\mathbf{R_D} = T_R \left[i x \tau \frac{\partial p}{\partial T} - \frac{1}{W} \frac{\partial W}{\partial T} x \frac{\partial}{\partial x} + \frac{\partial t_0}{\partial T} \frac{\partial}{\tau \partial x} \right]. \tag{37}$$

With the response of the absorber (14), as discussed in Section III, we can compute the shifts in the collective variables of the soliton per round-trip due to the saturable absorber according to (33)–(36)

$$\tilde{q}_s(W) = q_0 h_w\left(\epsilon, \frac{W}{E_A}\right) \tag{38}$$

$$\tilde{p}_s(W) = \frac{\alpha q_0}{\tau} h_p\left(\epsilon, \frac{W}{E_A}\right) \tag{39}$$

$$\tilde{\theta}_s(W) = -\alpha q_0 h_\theta\left(\epsilon, \frac{W}{E_A}\right) \tag{40}$$

$$\tilde{t}_s(W) = \tau q_0 h_t\left(\epsilon, \frac{W}{E_A}\right). \tag{41}$$

The auxiliary functions h_w, h_p, h_θ, and h_t are defined by

$$h_w(\epsilon, y) = \frac{1}{2q_0} \int_{-\infty}^{\infty} q_s(\epsilon, y) \operatorname{sech}^2(x)\, dx \tag{42}$$

$$h_p(\epsilon, y) = \frac{1}{q_0} \int_{-\infty}^{\infty} q_s(\epsilon, y) \tanh(x) \operatorname{sech}^2(x)\, dx \tag{43}$$

$$h_\theta(\epsilon, y) = \frac{1}{q_0} \int_{-\infty}^{\infty} q_s(\epsilon, y)[1 - x \tanh(x)] \operatorname{sech}^2(x)\, dx \tag{44}$$

$$h_t(\epsilon, y) = \frac{1}{q_0} \int_{-\infty}^{\infty} q_s(\epsilon, y) x \operatorname{sech}^2(x)\, dx. \tag{45}$$

In the limit of a very slow absorber ($\epsilon = 0$), we obtain the analytical results

$$h_w(0, y) = \frac{1}{y}[1 - \exp(-y)] \tag{46}$$

and

$$h_p(0, y) = \left(\frac{2}{y}\right)^2 \left\{1 - \exp(-y) - \frac{y}{2}[1 + \exp(-y)]\right\}. \tag{47}$$

The auxiliary functions are evaluated in Fig. 4(a)–(d). Note, if there is only an absorption change associated with the saturable absorber, $\alpha = 0$, then there is no shift in frequency and phase of the soliton due to the absorber. The reduced loss seen by the soliton, $\tilde{q}_s < q_0$, favors the soliton against the continuum, i.e., the background radiation, which will be the subject of the next sections. The continuous timing shift $\tilde{t}_s$ which is due to the fact that during each round-trip only the front part of the soliton is absorbed in case of a slow saturable absorber, has also a stabilizing function for the soliton, as will be discussed in more detail later on.

If the linewidth enhancement factor α is not zero, then there is an additional frequency shift of the soliton per round-trip due to the response of the absorber. This is the Raman self-frequency shift (RSFS) as has been observed for ultrashort pulses in fibers [42], [43]. The Raman shift is due to the asymmetric response of the refractive index and therefore vanishes for a instantaneous Kerr effect, $\epsilon \to \infty$. As we will see later, the RSFS can have a destabilizing as well as a stabilizing effect on the soliton.

Before we start to investigate the soliton stabilization mechanisms in more detail, we further simplify the evolution equations of the soliton variables and the continuum. In [38], we have shown that the coupling of the continuum to the soliton due to the finite gain and loss bandwidth can be neglected as long as the spectral width of the soliton is much smaller than the gain and loss bandwidth. In the case of strong saturation of the slow absorber, ($T_A \gg \tau$ and $W \gg E_A$), also the absorber only weakly couples the continuum to the soliton. Therefore, we neglect these coupling terms in the following, (see Appendix A). Furthermore, for the stability considerations later on, we will always assume that the system of equations is close to equilibrium, $dW/dT \approx dp/dT \approx 0$. Thus, terms like

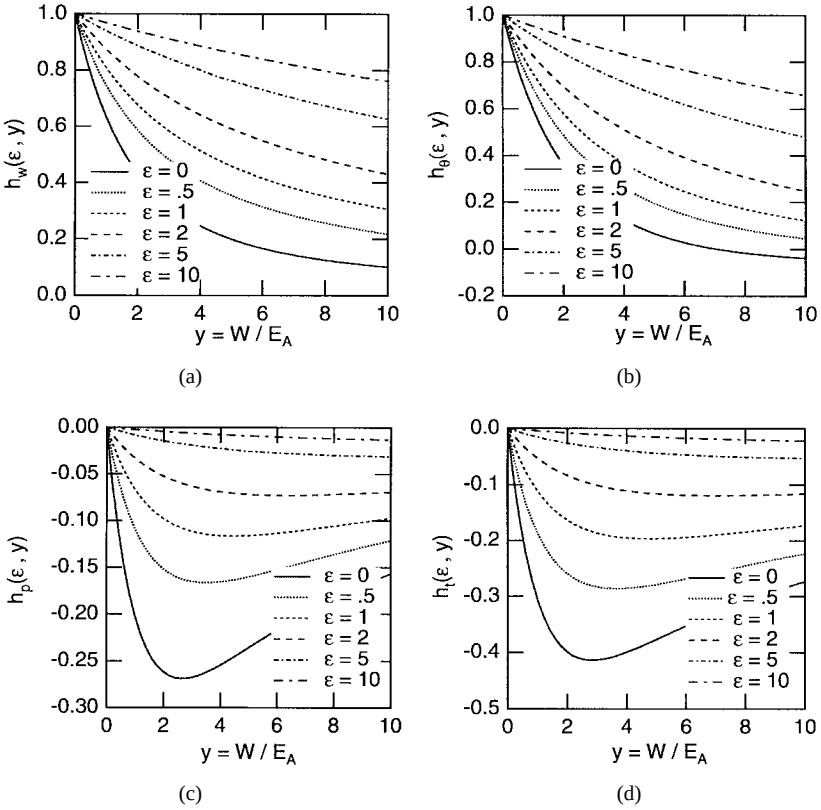

Fig. 4. (a) Normalized energy loss, (b) normalized phase shift, (c) normalized timing, and (d) normalized frequency shift per round-trip due to a saturable absorber for different ratios between pulsewidth and absorber recovery time ϵ.

dW/dTa_c can be considered as higher order terms and will be neglected in the following. This simplifies the operator $\mathbf{R_D}$ to

$$\mathbf{R_D} = T_R \frac{\partial t_0}{\partial T} \frac{\partial}{\tau \partial x}. \tag{48}$$

Using the approximations derived in Appendix A, the evolution equations for the soliton variables are

$$T_R \frac{\partial W}{\partial T} = 2\left[g - l - \frac{D_{g,f}}{3\tau^2} - D_{g,f} p^2 - \tilde{q}_s(W)\right] W \tag{49}$$

$$T_R \frac{\partial p}{\partial T} = -\frac{4}{3} \frac{D_{g,f}}{\tau^2} p + \tilde{p}_s(W) \tag{50}$$

$$T_R \frac{\partial t_0}{\partial T} = \tilde{t}_s(W) \tag{51}$$

$$T_R \frac{\partial \theta_0}{\partial T} = \tilde{\theta}_s(W). \tag{52}$$

Introducing the normalized group delay mismatch $T_{g,c}$ between the soliton and the continuum

$$T_{g,c} = 2\Phi_0 p\tau - \frac{\tilde{t}_s(W)}{\tau} \tag{53}$$

we obtain for the time evolution of the continuum,

$$T_R \frac{\partial g(k)}{\partial T} = -i[\tilde{\Phi}_0 + \Phi_0 k^2 + T_{g,c} k] + \langle \mathbf{f}_k^{(+)} | \mathbf{R}\mathbf{a}_c \rangle + \langle \mathbf{f}_k^{(+)} | \mathbf{R}\mathbf{a}(x) e^{-ipt} \rangle. \tag{54}$$

By inverse Fourier transformation of (54) we obtain for Gordons associated function

$$T_R \frac{\partial G(T,t)}{\partial T} = \left[g - l - i\tilde{\Phi}_0 + t_{g,c} \frac{\partial}{\partial t} + \overline{D} \frac{\partial^2}{\partial t^2} - q_s(t)\right] G(T,t) + \mathcal{F}^{-1}\left\{\langle \mathbf{f}_k^{(+)} | \mathbf{R}\mathbf{a}(x) e^{-ipt} \rangle\right\} \tag{55}$$

where $\overline{D} = D_{g,f} - iD$ is the complex dispersion in the system and $t_{g,c} = T_{g,c}\tau$, the group delay mismatch between soliton and continuum due to the nonlinearity.

A. Stationary Solution

Equations (49) and (50) imply that the laser reaches steady state when the saturated gain equals the losses experienced by the solitary pulse

$$g = l + \frac{D_{g,f}}{3\tau^2} + D_{g,f} p_0^2 + \tilde{q}_s(W_0) \tag{56}$$

with

$$g = \frac{g_0}{1 + \dfrac{W_0}{E_L}} \tag{57}$$

and

$$p_0 = -\frac{3}{4} \frac{\tau^2}{D_{g,f}} \tilde{p}_s(W_0). \tag{58}$$

Here, W_0 and p_0 are the steady-state pulse energy and center frequency of the soliton, respectively. Together with the

relation between soliton width and energy $\tau = 4|D|/\delta W_0$, (56) and (58) determine the steady-state pulse energy W_0 and center frequency p_0. We eliminate the Raman self-frequency shift from (56) via (58) and obtain an equation that determines the steady-state pulse energy directly

$$g = l + \frac{D_{g,f}}{3\tau^2} + \frac{9}{16}\frac{\tau^4}{D_{g,f}}\tilde{p}_s(W_0)^2 + \tilde{q}_s(W_0). \tag{59}$$

Usually one uses very moderate amounts of saturable absorption to mode-lock a laser, e.g., $q_0 \approx 1\%$ and total linear losses $l \approx 10\%$. As we will see later the filter losses of the pulse are smaller than the maximum modulation depth of the absorber, $D_{g,f}/3\tau^2 \leq q_0$. If there is no excessive linewidth enhancement factor the pulse energy is then approximately determined by

$$g = \frac{g_0}{1 + \dfrac{W_0}{E_L}} = l. \tag{60}$$

If the saturable absorption q_0 is comparable with the frequency independent loss l, or if the absorber has a large linewidth enhancement factor one has to solve (59) numerically and it can possess multiple solutions. In general, these solutions depend in a complex way on the system parameters and they will be studied in more detail elsewhere.

Equations (51) and (52) indicate that the timing and phase shifts increase with the additional rates $\tilde{t}_s$ and $\tilde{\theta}_s$. As we will see later, the timing shift is important for the stability of the continuum. Once the soliton energy and momentum are fixed one can compute from (55) the steady-state continuum contribution which we assume to remain small even in steady state. However, this is only true if the values for the soliton parameters and the continuum are stable.

B. Stability of the Stationary Solution

As we have seen in the preceding sections the coupling of the continuum back to the soliton due to gain dispersion and saturable absorption can be neglected. Therefore, the equations of motion for the soliton variables are decoupled from the continuum, i.e., background radiation, so that we can study the stability of the four soliton variables and the continuum separately.

1) Stability of the Soliton Variables: We consider the dynamics in the subspace of the four soliton variables according to (49) and (50). Since the timing and phase shifts of the soliton do not couple back to energy and momentum of the soliton, it is enough to investigate the stability of energy and momentum of the soliton. To keep the discussion short we consider the case where we can neglect the finite gain bandwidth so that the laser bandwidth is completely determined by the bandwidth of an intracavity filter, which can be the finite bandwidth of the cavity mirrors, i.e., $D_{g,f} = D_f = 1/\Omega_f^2$. We introduce the normalized soliton energy $y = W/E_A$ and momentum $x = p\sqrt{D_{g,f}/l}$ and rewrite the dynamics on a time scale of the cavity decay time $t' = T \cdot l/T_R$

$$\frac{\partial y}{\partial t'} = 2[g_n(y) - 1 - s h_w(\epsilon, y) - \frac{1}{3}f^2y^2 - x^2]y \tag{61}$$

$$\frac{\partial x}{\partial t'} = -\frac{4}{3}f^2y^2\left[x - \frac{3}{4}\frac{\alpha s}{f}\frac{h_p(\epsilon, y)}{y}\right] \tag{62}$$

with the normalized saturated gain $g_n(y) = g/l = r/(1+\chi y)$. The normalization reduces the number of free parameters. The following five dimensionless parameters remain.

Filter Strength:

$$f = \frac{\delta E_A}{\Omega_f 4|D|}. \tag{63}$$

Normalized Saturable Absorption:

$$s = \frac{q_0}{l}. \tag{64}$$

Saturation Factor:

$$\chi = \frac{E_A}{E_L}. \tag{65}$$

Pump Parameter:

$$r = \frac{g_0}{l}. \tag{66}$$

Normalized Ratio Between Absorber Recovery Time and Pulsewidth:

$$\begin{aligned}\epsilon' &= \epsilon y \\ &= \frac{\tau}{\tau_A}y \\ &= \frac{4|D|}{\tau_A \delta E_A}.\end{aligned} \tag{67}$$

The filter strength f is the ratio between the change in the pulse spectrum, if the pulse energy is increased by the saturation energy of the absorber and the available laser bandwidth, Ω_f. The normalized saturable absorption s is the ratio between the saturable and the nonsaturable losses in the laser. The saturation factor is the ratio between the saturation energy of the absorber and the gain medium. The pump parameter r describes how many times the laser is above threshold in the absence of the saturable absorber. Thus the stationary normalized frequency shift x_s is given by

$$x_s = \frac{4}{3}\frac{\alpha s}{f}\frac{h_p\left(\dfrac{\tilde{\epsilon}}{y}, y\right)}{y}. \tag{68}$$

Equation (68) shows that the Raman self-frequency shift becomes large for low filter strength. Fig. 5 shows the normalized steady-state frequency shift as a function of the normalized pulse energy for different normalized ratios between absorber recovery time and pulsewidth ϵ'. Thus, for a fast absorber, i.e., large ϵ', the laser shows no RSFS. However, for a slow absorber, i.e., small ϵ', a considerable RSFS can occur.

Instead of solving the remaining equation (61) for the missing steady-state energy y_s, we can express the necessary

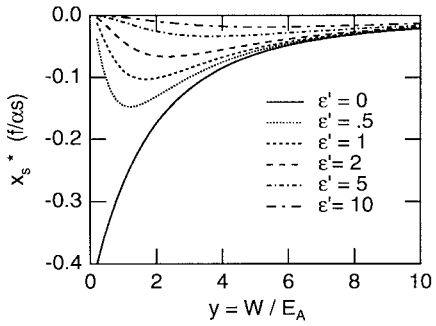

Fig. 5. Normalized steady-state frequency shift as a function of normalized pulse energy for different values of the normalized ratio between absorber recovery time and pulsewidth ϵ'.

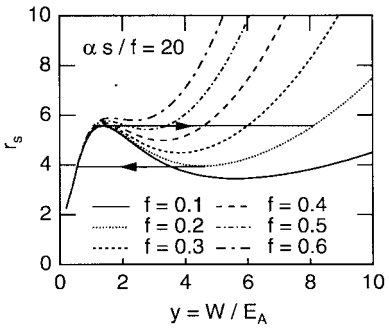

Fig. 6. Necessary pump parameter as a function of the normalized pulse energy for $s = 1$, a constant product $\alpha s/f = 20$, and $\epsilon' = 1$ for different filter strength *f*.

pump parameter, r_s, as a function of the steady-state pulse energy

$$r_s = (1+\chi y)\left\{1 + sh_w\left(\frac{\tilde{\epsilon}}{y}, y\right) + \frac{1}{3}f^2y^2 + \frac{9}{16}\left[\frac{\alpha s}{f}\,\frac{h_p\left(\frac{\tilde{\epsilon}}{y}, y\right)}{y}\right]^2\right\}. \tag{69}$$

Fig. 6 shows the necessary pump parameter for $s = 1$, a constant product $\alpha s/f = 20$ and $\epsilon' = 1$ for different filter strength. The parameter range where a large RSFS occurs requires a very high pumping rate since a possible pulse is shifted into the wing of the filter. The RSFS leads to a maximum overshoot of the pump parameter for a pulsewidth of the order of the absorber recovery time where it is strongest. Linearization of (61) to (62) results in

$$T_R\frac{\partial \Delta y}{\partial T} = \alpha_{11}\Delta y + \alpha_{12}\Delta x \tag{70}$$

$$T_R\frac{\partial \Delta x}{\partial T} = \alpha_{21}\Delta y + \alpha_{22}\Delta x \tag{71}$$

where the coefficients α_{ij} are given by

$$\alpha_{11} = 2\left[\frac{\partial g_n}{\partial y} - sh_w'(y) - \frac{2}{3}f^2y\right]y \tag{72}$$

$$\alpha_{12} = -3\frac{\alpha s}{f}\,h_p(y) \tag{73}$$

$$\alpha_{21} = -3\alpha f s[h_p(y) + h_p'(y)y] \tag{74}$$

$$\alpha_{22} = -\tfrac{4}{3}f^2y^2. \tag{75}$$

The stationary values are stable, if the trace of the coefficient matrix is negative and its determinant is positive

$$\text{i)}\quad \alpha_{11} + \alpha_{22} < 0 \tag{76}$$

$$\text{ii)}\quad \alpha_{11}\alpha_{22} - \alpha_{12}\alpha_{21} > 0. \tag{77}$$

The coefficient α_{22} is always negative. Also the coefficient α_{11} is negative if the ratio between saturable and nonsaturable losses is not too large. By partial derivation of the stationary equations (61) and (62), it can be shown

$$\frac{\partial r_s}{\partial y} = -\frac{1+\chi y}{\alpha_{22}}(\alpha_{11}\alpha_{22} - \alpha_{12}\alpha_{21}). \tag{78}$$

Equation (78) shows, that for a given pump parameter in Fig. 6, only those values for the pulse energy can be stable (and, therefore, physically accessible), which are on the positive slope of the curve. This behavior may lead to a suppression of short pulses, and a hysteresis in the output power versus pump parameter curve, see Fig. 6. The phase modulation due to a slow refractive index change can effectively prohibit self-starting mode-locking, if the laser can not be pumped strong enough to overcome the RSFS.

2) Stability of the Continuum: However, for a successful mode-locked operation, additional conditions arise from the stability of the continuum. The continuum is stable, if all the eigenmodes of the evolution operator of the homogeneous part of (55) experience net loss per round-trip. Thus, we have to study the eigenvalue problem

$$\lambda_n G_n(t) = \left[g - l - i\tilde{\Phi}_0 + t_{g,c}\frac{\partial}{\partial t} + \overline{D}\frac{\partial^2}{\partial t^2} - q_s(t)(1+i\alpha)\right]G_n(t). \tag{79}$$

The real part of the eigenvalue λ_n is the gain and the imaginary part is the phase shift per round-trip experienced by the nth eigenmode. The continuous timing shift $t_{g,c}$ describes the difference in group delay between the soliton and the continuum. This timing shift can be removed by the following transformation

$$G_n(t) = H_n(t)\,\exp\left[-\frac{t_{g,c}}{2\overline{D}}\,t\right] \tag{80}$$

which results in the new eigenvalue problem

$$\tilde{\lambda}_n H_n(t) = \left[\overline{D}\frac{\partial^2}{\partial t^2} - q_s(t)(1+i\alpha)\right]H_n(t) \tag{81}$$

with the total eigenvalue

$$\lambda_n = g - l - \frac{t_{g,c}^2}{4\overline{D}} + \tilde{\lambda}_n. \tag{82}$$

The mathematical elimination of the first-order term in (79) results in the additional loss term in (81). Physically, this

means that the group delay mismatch between the continuum and the soliton leads to an additional loss for the continuum eigenmodes since the continuum once generated drifts continuously away from the window of minimum loss. This mechanism leads to a stabilization of the soliton against the continuum by introducing the additional continuum loss

$$l_{c,\,\mathrm{shift}} = \mathrm{Re}\left\{\frac{t_{g,\,c}^2}{4\overline{D}}\right\} = \frac{t_{g,\,c}^2}{4D_{g,\,f}(1+D_n^2)}. \tag{83}$$

The importance of this stabilization mechanism becomes obvious when we compare the additional continuum loss due to shifting between soliton and continuum, with the soliton loss due to bandwidth limitation. We obtain with (53)

$$\begin{aligned}\frac{l_{c,\,\mathrm{shift}}3\tau^2}{D_{g,\,f}} &= \frac{3}{4}\frac{\phi_0^2}{\phi_0^2+\left(\frac{D_{g,\,f}}{\tau^2}\right)^2}\left(\frac{T_{g,\,c}}{\phi_0}\right)^2 \\ &= \frac{3}{4}\frac{\phi_0^2}{\phi_0^2+\left(\frac{D_{g,\,f}}{\tau^2}\right)^2}\left(2p_0\tau-\frac{\tilde{t}_s}{\phi_0\tau}\right)^2 \\ &= \frac{3}{4}\frac{\phi_0^2}{\phi_0^2+\left(\frac{D_{g,\,f}}{\tau^2}\right)^2} \\ &\quad\cdot\left[2\alpha h_p(\epsilon,\,y)-\frac{q_0}{\phi_0}\,h_t(\epsilon,\,y)\right]^2. \end{aligned}\tag{84}$$

Soliton perturbation theory is only a good approximation if the phase shift per round-trip is much bigger than the filter loss and the pulse shaping due to the saturable absorber, i.e., $\phi_0 \gg D_{g,\,f}/\tau^2$. Thus, we can approximate (84) by

$$I_{c,\,\mathrm{shift}} \approx \frac{D_{g,\,f}}{\tau^2}\left[p_0\tau-\frac{q_0}{2\phi_0}\,h_t(\epsilon,\,y)\right]^2. \tag{85}$$

Equation (85) shows that the continuum loss induced due to the group delay mismatch between the soliton and the continuum can be as large as the filter loss experienced by the soliton. The effect is maximum if we saturate the absorber such that the RSFS and the timing shift due to the front absorption of the soliton add up. Fig. 4(c) and (d) show that this is the case for a pulse energy about 2–3 times the saturation energy of the absorber, i.e., $y = 2-3$. Furthermore, the two effects add up if the linewidth enhancement factor α is negative, i.e., the refractive index change is negative.

Before we discuss the continuum loss due to the group delay mismatch between soliton and continuum in further detail, we complete the study of the stability issues involved with the continuum by investigating the eigenvalue spectrum of the reduced continuum (81) in two different approximations, (see Fig. 7).

i) by a V-shaped response:

$$q_s(t) = q_0 + \hat{q}_0\left(\frac{t}{\tau_A}-1\right), \quad \text{for } t>0 \text{ and } \infty \text{ for } t<0.$$

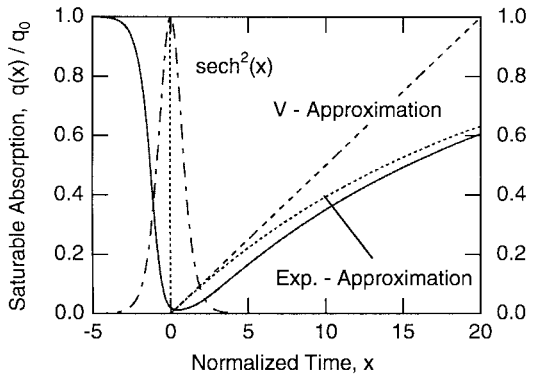

Fig. 7. Different approximations for the absorber response.

ii) by an exponential response:

$$q_s(t) = q_0 - \hat{q}_0\,\exp\left[-\frac{t}{\tau_A}\right], \quad \text{for } t>0 \text{ and } q_0 \text{ for } t<0. \tag{86}$$

1) V-Shaped Response: For the V-shaped approximation of the response we obtain from (81) a standard eigenvalue problem for a Schrödinger operator with complex coefficients. According to the perturbation theory for linear operators the eigenvalues have a unique analytic continuation into the complex plain. The V-potential is a standard problem solved in [49]. We obtain with the eigenvalue for the ground state

$$\begin{aligned}\tilde{\lambda}_0 &= -(1+i\alpha)\left(q_0-\hat{q}_0\left\{1-2.338\right.\right. \\ &\qquad\left.\left.\cdot\left[\frac{\overline{D}}{\hat{q}_0(1+i\alpha)\tau_A^2}\right]^{1/3}\right\}\right) \\ &= -(1+i\alpha)\left(q_0-\hat{q}_0\left\{1-2.338\right.\right. \\ &\qquad\left.\left.\cdot\left[\frac{\frac{1}{D_n}+i}{(1+i\alpha)^2}\right]^{1/3} w_A^{-2/3}\right\}\right) \end{aligned}\tag{87}$$

where

$$w_A = \frac{\tau_A}{\tau}\sqrt{\frac{\hat{q}_0}{\phi_0}} \tag{88}$$

denotes the normalized absorber recovery time. For the case of a strongly saturated absorber, $\hat{q}_0 = q_0$, we obtain for the loss of the most unstable continuum mode normalized to the maximum saturable absorption

$$\begin{aligned}\frac{l_{c,\,stat}}{q_0} &= -\mathrm{Re}\left\{\frac{\tilde{\lambda}_0}{q_0}\right\} \\ &= 2.338\left[\left(\frac{1}{D_n}+i\right)(1+i\alpha)^2\right]^{1/3} w_A^{-2/3}. \end{aligned}\tag{89}$$

Fig. 8 shows the normalized continuum losses as a function of the normalized recovery time w_A for a vanishing linewidth

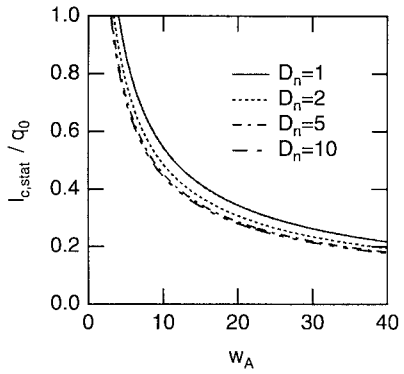

Fig. 8. Normalized continuum losses as a function of the normalized recovery time w_A for vanishing linewidth enhancement factor $\alpha = 0$ and different values of the normalized dispersion. For small values of the normalized recovery time the calculated normalized continuum loss becomes larger than one, which is an artifact of the infinite V-potential approximation.

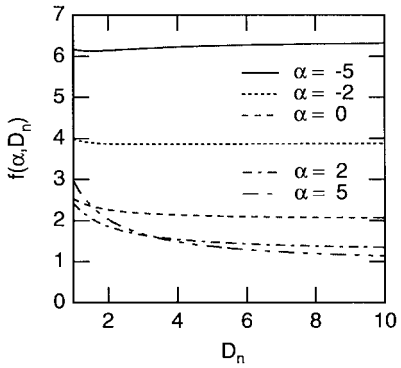

Fig. 9. Variation of the factor $f(\alpha, D_n)$ which scales the continuum losses as a function of the normalized dispersion and the linewidth enhancement factor α.

enhancement factor, $\alpha = 0$, and different values of the normalized dispersion. For small values of the normalized recovery time the calculated normalized continuum loss becomes larger than one, which is of course an artifact of the infinite V-potential approximation. For large normalized recovery times, the real parts of the eigenvalues lay deep in the V-potential, and therefore the used approximation gives the right asymptotic behavior for large w_A. Thus, we see, that even for a normalized recovery time as large as 40 almost 20% of the available saturable absorption is still left over as continuum losses which can stabilize a soliton against the continuum. Fig. 9 shows the variation of the forefactor

$$f(\alpha, D_n) = 2.338\left[\left(\frac{1}{D_n} + i\right)(1 + i\alpha)^2\right]^{1/3} \tag{90}$$

which scales the continuum losses as a function of the normalized dispersion and the linewidth enhancement factor α. The influence of the normalized dispersion onto the continuum loss is rather small if it is not chosen to be excessively large, as it is possible in actively mode-locked systems [38]. The analytic result (90) shows, that the continuum losses scale with the inverse third root of the normalized dispersion. This explains the weak dependence on the normalized dispersion. However, a phase modulation due to a nonvanishing linewidth enhancement factor is important. The forefactor (90) scales with the power 2/3, almost linearly. A positive linewidth enhancement factor, which corresponds to a refractive index increase during saturation, leads to a destabilization of the continuum. This can be understood by the modulational instability that exists in a medium with negative dispersion and positive Kerr effect in the presence of a pump [39]. Here, the pump is the soliton. If the linewidth enhancement factor is negative, which corresponds to a negative Kerr effect, no modulational instability is present. In this case, the additional phase modulation leads to an additional spreading of the continuum in the frequency domain and therefore pushes the continuum into the region of higher filter losses which results in additional continuum losses. Therefore, an ideal absorber for good mode-locking behavior should have a negative linewidth enhancement factor.

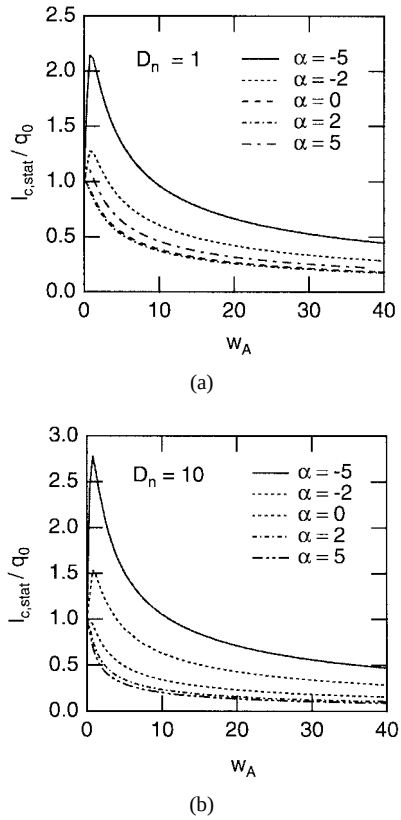

Fig. 10. Normalized continuum losses for a fully saturated absorber that recovers with an exponential response as a funtion of the normalized recovery time and the linewidth enhancement factor α: (a) for a normalized dispersion $D_n = 1$ and (b) for a normalized dispersion $D_n = 10$.

2) Exponential Response: The analytic solution of the eigenvalue problem for the complex exponential response is presented in Appendix B. Fig. 10(a) and (b) show the resulting normalized continuum losses for a fully saturated absorber as a function of the normalized recovery time for two different values of the normalized dispersion. Comparison with the results obtained for the V-potential shows that the V-approximation and the results for the exponential potential agree rather well for a normalized recovery time larger than 10. Again, the continuum loss only weekly depends on the normalized dispersion. Fig. 10 clearly demonstrates again that

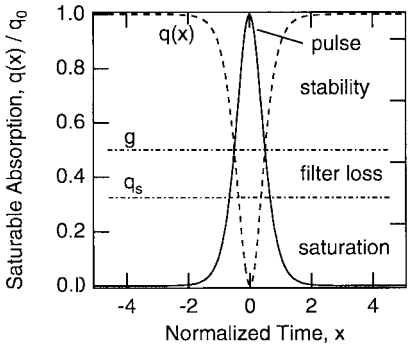

Fig. 11. Gain and loss balance in a laser mode-locked by a fast saturable absorber only.

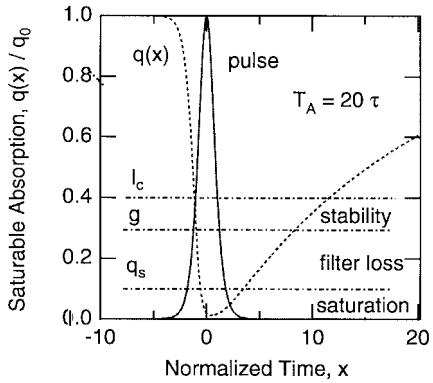

Fig. 12. Gain and loss balance in a soliton mode-locked laser stabilized by a slow saturable absorber.

a negative linewidth enhancement factor increases stability. With an absolute value for the linewidth enhancement factor as large as 5 the effective continuum loss increases almost by a factor of 4. Such large negative linewidth enhancement factors are possible, for example, near the band edge in bulk GaAs [46]–[48] for quasi-CW excitation. The normalized recovery time w_A is not simply the ratio between the absorber recovery time and the pulsewidth but is in addition multiplied by the square root of the ratio between saturable absorption and the nonlinear phase shift. As we will see later the nonlinear phase shift can be as large as 0.5 whereas the saturable absorption is typically on the order of 0.5%–5%. Therefore, the normalized recovery time w_A can be a factor of 3–10 smaller than the actual value of τ_A/τ. Thus, we can still use a large fraction of the saturable absorber action to overcome the bandwidth limitation in a mode-locked laser while we use a saturable absorber with a relaxation time 10–30 times longer than the pulsewidth achieved. This is the most striking feature of soliton-mode-locked lasers. Traditional laser models [25] provide stability for the single pulse solution by dissipative mechanisms that generate a short net gain window in time that supports only the pulse. Fig. 11 shows the gain and loss balance for the fast saturable absorber mode-locking model. The gain and loss curves cross each other exactly at the full width half maximum points. In contrast, Fig. 12 shows the situation for a soliton mode-locked laser, where the pulsewidth τ is ten times shorter than

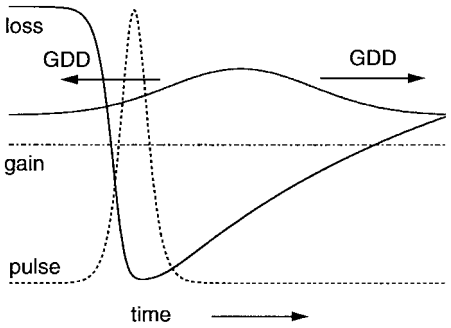

Fig. 13. Spreading of the continuum in the net gain window due to dispersion.

the absorber recovery time, and the pulse energy is ten times the saturation energy. During saturation of the absorber, the soliton experiences already 10% of the absorber losses per round-trip. According to Fig. 10 the continuum experiences up to 30% of the available absorption as loss, even if the absorber has a vanishing linewidth enhancement factor. Then, one can use almost all of the remaining 20% of the absorption to overcome the bandwidth limitation and to provide still some stability against the growth of continuum. Thus, there is a considerable open net gain window when compared with the fast saturable absorber mode-locking scheme but the pulse is still stable against the growth of continuum. This is possible in a soliton mode-locked laser, because the pulse is shaped by a balance between negative GDD and SPM. In contrast, the weak background radiation, the continuum, only experiences the linear effects, especially the dispersion, (see Fig. 13).

C. Discussion of Different Stabilization and Pulse Cleaning Mechanisms

In total, we obtain for the round-trip gain of the continuum, the real part of the eigenvalue of the most unstable continuum mode, from (56), (79), (80), and (85)

$$\mathrm{Re}\{\lambda_0\} = l_s - l_c \tag{91}$$

where

$$l_s = \frac{D_{g,f}}{3\tau^2} + D_{g,f}p_0^2 + \tilde{q}_s(W_0) \tag{92}$$

is the soliton loss due to the finite laser bandwidth, the RSFS and the saturable absorber. The round-trip loss of the most unstable continuum mode is given by

$$\begin{aligned} l_c &= l_{c,\mathrm{shift}} + l_{c,\mathrm{stat}} \\ &\approx \frac{D_{g,f}}{\tau^2}\left[p_0\tau - \frac{q_0}{2\phi_0}h_t(\epsilon, y)\right]^2 + l_{c,\mathrm{stat}}. \end{aligned} \tag{93}$$

The soliton is stable, if the lowest order continuum mode decays, $\mathrm{Re}\{\lambda_0\} < 0$, i.e.,

$$l_s < l_c. \tag{94}$$

The first part of the continuum loss is due to the group delay mismatch between soliton and continuum, and the second part due to the finite gain bandwidth and the saturable absorption. If we neglect for the moment the direct timing shift due to

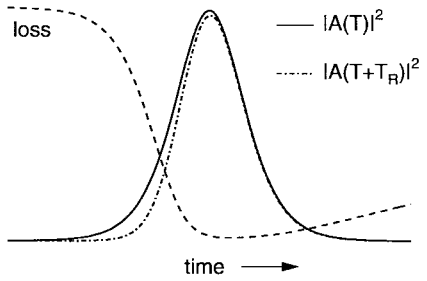

Fig. 14. Due to the asymmetric response of a slow absorber, the soliton is continuously shifted against the continuum.

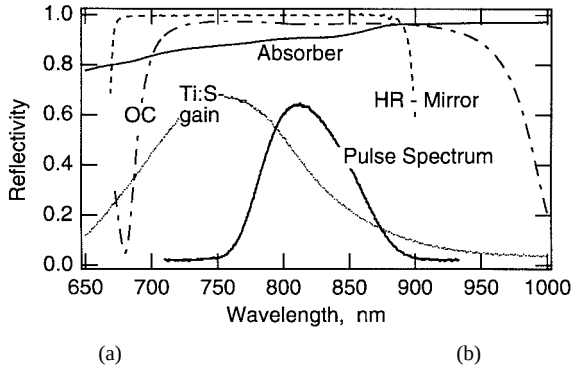

Fig. 15. Spectrum of the soliton mode-locked pulse, reflectivity of the mirrors and the measured fluorescence of Ti:sapphire.

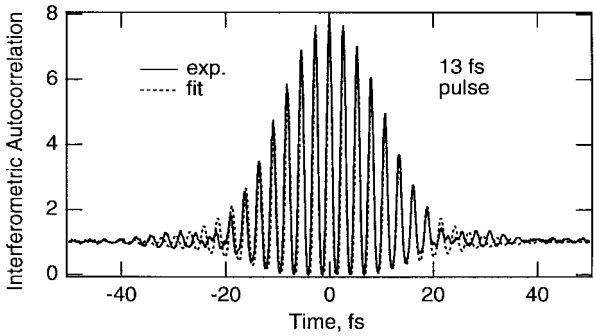

Fig. 16. Measured interferometric autocorrelation trace of the 13-fs soliton mode-locked pulse.

the slow saturable absorption, (92) to (93) indicate that the losses for the soliton due to the RSFS are as large as the additional losses experienced by the continuum due to the difference in group delay via the RSFS. Thus, a RSFS is of no help in stabilizing the soliton against the continuum. However, the direct shift of the soliton due to the slow absorption leads to a continuous retardation of the soliton against the continuum generated by the perturbations onto the soliton. Once separated from the soliton the continuum is absorbed by the unsaturated absorber is now in front of the soliton. This is an additional pulse stabilization and cleaning mechanism not present in a fast saturable absorber. The mechanism is very similar to the sliding frequency filter technique invented by Linn Mollenauer. There, the center frequency of the filter is continuously shifted, so that the soliton can follow the center frequency of the filter but the continuum cannot. Then, the continuum is on the average absorbed in the stop band of the filter. In the case of a slow saturable absorber this happens in the time domain, (see Fig. 14). Due to the continuous retardation of the soliton with respect to the continuum, the continuum experiences an average additional loss given by the term in (93). If the ratio between the absorption and the nonlinear phase shift is not larger than one, which is hardly the case, the soliton shifting cannot provide much stability to the pulse and the pulse stability is mainly determined by the real part of the eigenvalue in the stationary potential $l_{c,\mathrm{stat}}$.

V. Experimental Results

The main result of the previous section is, that we can stabilize pulse formation in a mode-locked laser by a saturable absorber with a response time about 10–20 times longer then the pulsewidth. With a given amount of saturable absorption one achieves almost the same performance as with an ideal fast saturable absorber due to soliton formation. Recently, we demonstrated experimentally the soliton mode-locking principle. We achieved pulses about 30 times shorter than the response time of the absorber. In this section, we present experimental results on the shortest pulses achieved so far with this technique.

We used a standard Ti:sapphire laser [30] with a 2-mm Ti:sapphire crystal and a 40-cm fused silica prism sequence. To make the absorber broad band, we processed a LT-GaAs absorber layer on a silver mirror [30]. With this setup, we achieved pulses as short as 13 fs, (Figs. 15 and 16) over the full stability range of the cavity, when the mirror supporting the absorber is moved. This is in sharp contrast to operation of the laser in KLM mode, when the absorber mirror is replaced with a normal high reflector. Then the laser shows only mode-locking over a very small fraction of the stability range of the cavity.

The pulse spectrum has a FWHM of about 73 nm with its center frequency at 810 nm. The pulse spectrum extends from the absorption edge at 870 nm to about 770 nm, where it can saturate the absorber most efficiently and where the absorption is flat over the wavelength. Fig. 17 shows the pump-probe response of the LT-GaAs semiconductor absorber mirror at 810 nm when excited with 10-fs pulses with a pulse energy fluence similar to the intracavity fluences when used to mode-lock the laser. The pump-probe trace well resolves the 60-fs carrier thermalization time for undoped GaAs as measured previously by Knox [45] with differential transmission measurements. Thus the pulse is about four times shorter than the fastest recovery time of the absorber. The pulse could not be tuned to shorter wavelength without broadening or breaking up into multiple pulses. Nevertheless, this is a pulsewidth which was previously only achievable by KLM. Fig. 18 shows the mode-locking build-up behavior of the laser. First the laser starts CW-running. After about 200 μs, the pulses build up and saturate the absorber. Therefore, the average output power almost doubles. Thus, the laser is truly self-starting. Further optimization of the absorber and a better understanding of the saturation behavior, phase effects and possible coherent effects [40], [41] in this absorber on a ten femtosecond time scale will help to improve these first results.

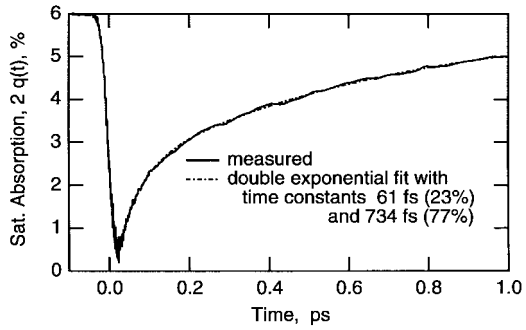

Fig. 17. Pump-probe trace of the LT-GaAs semiconductor absorber mirror at 810 nm with 10-fs pulses. The pump-probe trace well resolves the 60-fs carrier thermalization time for undoped GaAs.

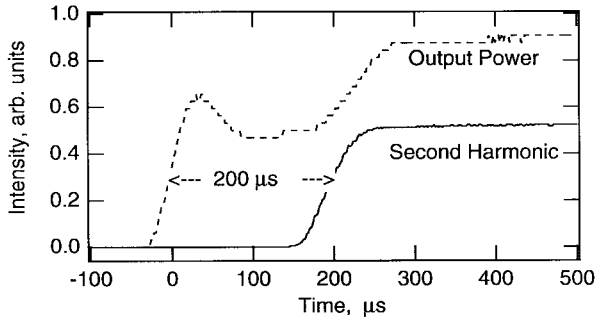

Fig. 18. Measured mode-locking buildup behavior of the 13-fs soliton mode-locked pulse.

TABLE I
PARAMETERS USED FOR NUMERICAL SIMULATIONS

Parameter	Value
l	0.025
g_0	0.07
P_L	3.2 W
Ω_g	$2\pi\cdot$ 43 THz
δ	0.4/MW
$q_{0,1}$	0.01
$T_{A,1}$	60 fs
$E_{A,1}$	4 nJ
$q_{0,2}$	0.02
$T_{A,2}$	734 fs
$E_{A,2}$	4 nJ

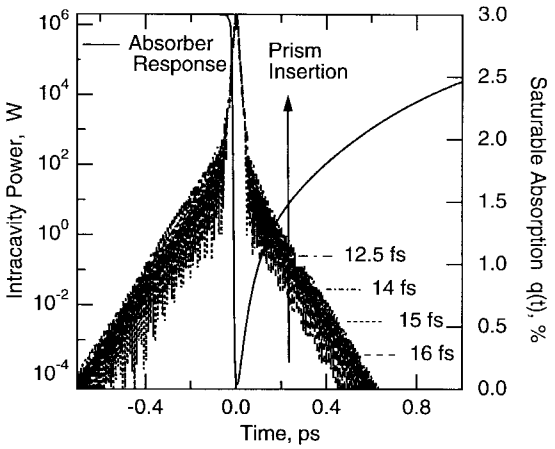

Fig. 20. Intensity and saturable absorption for increasing prism insertion. The simulation is with the parameters listed in Table I and an additional linewidth enhancement factor of $\alpha = -2$ for both absorbers.

VI. NUMERICAL SIMULATIONS

Since we extracted the most important absorber parameters by independent pump-probe measurements, we can compare the experimentally achieved results with the numerical simulations on the basis of the master equation (1). The simulations are done using the split-step Fourier transform method, where the SPM and the total intracavity dispersion per round-trip is applied in one step very much as it occurs in the real laser. The semiconductor absorber dynamics is modeled by two saturable absorbers obeying (3) with the parameters collected in Table I. The reflectivity of the mirrors, the transmission of the output couplers and the actual group delay dispersion due to the prisms is included in the simulation. The laser is simulated for different prism insertions, which results in different values for the dispersion and also higher order dispersion, Fig. 19(d). Fig. 19(a) shows the absorber response when saturated by the pulse, which stays very much the same for all simulations. On top of the absorber response, the pulse power is shown for the different runs. With increasing prism insertion, the amount of negative dispersion is reduced and the pulse gets initially shorter, down to about 14 fs at FWHM. Then, in the window of net gain, the continuum starts to grow as expected. This leads to the formation of a pulse pedestal as shown more clearly in the autocorrelation traces of Fig. 19(b). Reducing the amount of negative dispersion even further, does not lead to shorter pulses. Instead more and more energy flows into the continuum for different reasons. First the impact of the third-order dispersion and also the discrete nature of the SPM and the dispersion in the cavity leads to an energy flow from the soliton to the continuum, i.e., increased soliton losses. Finally also the bandwidth limitation due to the finite mirror and gain bandwidth introduces soliton losses which limits the shortest pulses achievable, even if the higher order dispersion can be fully eliminated and the SPM is reduced. Fig. 19(c) shows the corresponding spectra. The spectra look very much like a sech-square until the continuum takes over, which consists of long pulses, therefore, narrow spectral components appear in the pulse spectrum. Note, the simulated pulse spectra are centered around a much shorter wavelength, close to the peak of the gain of Ti:Sapphire, in contrast to the experiment. This is easily understood, because we neglect in the simulation, the wavelength dependent losses occurring in the absorber. The losses of the absorber are clearly wavelength dependent, see Fig. 15, which pushes the spectrum to longer wavelength in the experiment.

We performed the same simulations with a linewidth enhancement factor of $\alpha = -2$. Fig. 20 shows the corresponding intensity profiles of the steady-state pulses for increasing prism insertion. We achieve now pulses as short as 12.5 fs and one clearly recognizes the much better continuum suppression for these even shorter pulses when compared with Fig. 19(a). This confirms that a negative linewidth enhancement factor of the absorber leads to additional losses for the continuum as derived theoretically in Section IV-B-2.

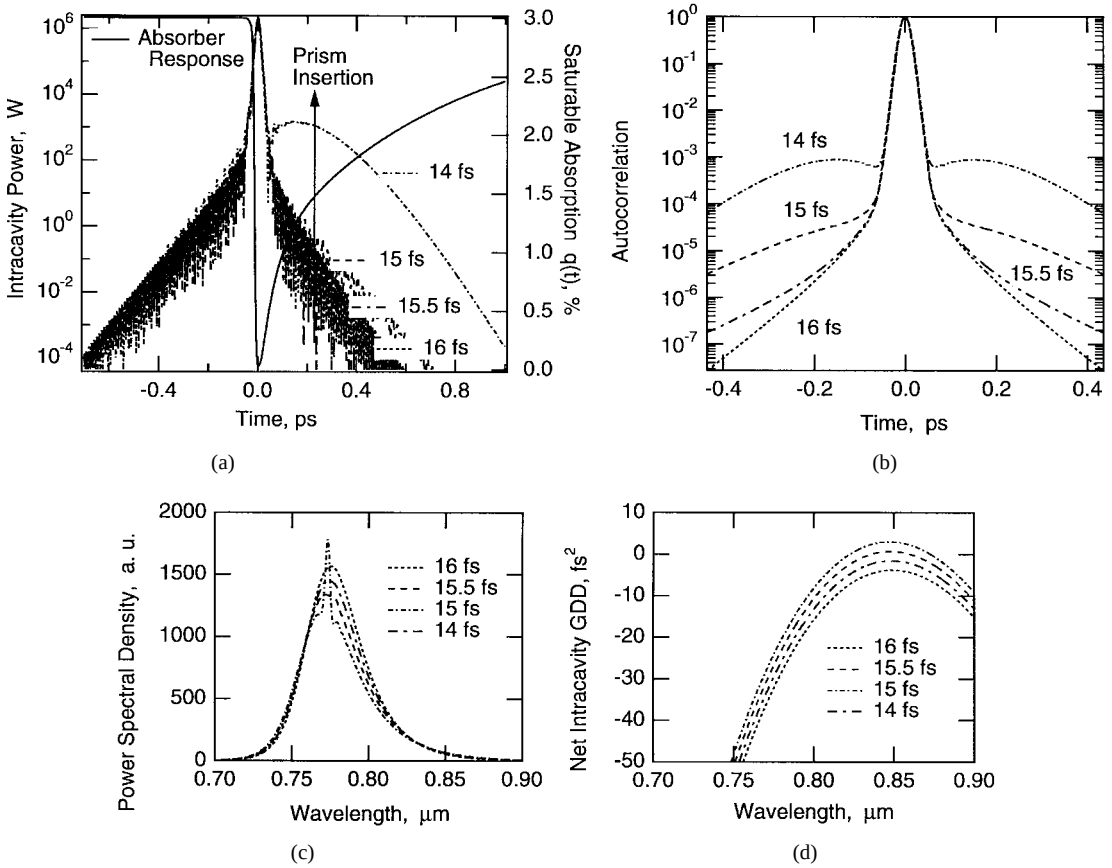

Fig. 19. (a) Intensity and saturable absorption for increasing prism insertion, (b) autocorrelation traces, (c) corresponding pulse spectra, and (d) net intracavity prism dispersion. The parameters used in the simulation are listed in Table I.

In total, the analytical and numerical results presented her, show that the independently measured pump probe response together with the assumption of a small negative linewidth enhancement factor and the soliton mode-locking principle is enough to explain the experimental results so far obtained.

VII. Conclusion

We have shown, that strongly saturated and relatively slow absorbers can be used to generate pulses much shorter than the recovery time of the absorber, if solitonlike pulse shaping is employed. This is a mode-locking principle distinct from the traditional schemes, that are based on an ideal fast saturable absorber, i.e., a fast saturable absorber that never saturates [31], or on the interplay between gain and loss saturation. In the soliton mode-locking scheme, the pulse shaping is completely done by the reversible effects GDD and SPM, which results in an almost Hamiltonian mode-locking [37] that is only stabilized by the saturable absorption. The unique properties of soliton systems, where the pulse is shaped by the nonlinear and the dispersive effects, whereas the background radiation only experiences the dispersive effects allows the use of slow saturable absorbers. As will be shown in more detail elsewhere, soliton formation not only allows us to achieve pulses about 10–20 times shorter than the recovery time of the absorber but in addition, we can achieve a pulsewidth comparable to a laser mode-locked by a fast saturable absorber given the same amount of saturable absorption for both cases. If the absorber shows in addition to the saturable absorption also a negative slow self-phase modulation that follows the absorption even better performance with respect to continuum suppression can be expected. Based on these results, we demonstrated theoretically and experimentally, that the fast time constants in semiconductor absorbers due to thermalization processes are fast enough to generate pulses in the 10-fs range, which was previously only possible by KLM. In contrast to KLM, we use real absorption and not artificial absorption generated via self-focusing. Thus, we have a decoupling between the laser modes and the laser dynamics and, therefore, we retain a much larger degree of freedom in the cavity design. This is extremely useful for high repetition rate, compact and diode-pumped lasers [44]. The slow time constant involved in semiconductor saturable absorbers due to carrier recombination, leads to a self-starting mode-locking process and a short mode-locking buildup time [50], [51], even for the shortest pulses. In addition, we have full freedom in designing the saturable absorption and the strength of the SPM, which might help in the long run to further shorten the pulses without overdriving the SPM.

Appendix A
Approximations for Soliton Perturbation Theory

In this Appendix, we prove the validity of some important approximations used for the interaction between soliton and continuum due to the response of a slow saturable absorber.

The absorber considered here is defined by (3). The parameter we consider to be small is the ratio between pulsewidth and absorber recovery time $\epsilon = \tau/\tau_A \ll 1$. Now, we show to lowest order in ϵ that the response of a slow absorber excited by a soliton does not introduce coupling of the continuum to the soliton and that the response is diagonal in the continuum representation. The response of the absorber can be written as

$$q(t) = q(\epsilon x). \tag{95}$$

The response can also be expressed in terms of its Fourier transform

$$q(\epsilon x) = \int_{-\infty}^{\infty} \tilde{q}(\omega) e^{-i\omega\epsilon x}\, d\omega. \tag{96}$$

When computing the matrix elements of the perturbation in the continuum representation we have to evaluate terms like

$$\langle \mathbf{f}_{k_1}^{(+)} | q(\epsilon x) | \mathbf{f}_{k_2} \rangle = \int_{-\infty}^{\infty} d\omega \tilde{q}(\omega) \langle \mathbf{f}_{k_1}^{(+)} | e^{-i\omega\epsilon x} | \mathbf{f}_{k_2} \rangle. \tag{97}$$

From the expression for the continuum eigenfunctions equation (2.35) from [38] we obtain

$$e^{-i\omega\epsilon x}|\mathbf{f}_{k_2}> = \Big| \mathbf{f}_{k_2-\omega\epsilon} > + \epsilon\omega e^{i(k_2-\omega\epsilon)x} \cdot \{2[k_2 + i\,\tanh(x)] + \omega\epsilon\} \Big| \begin{pmatrix} 1 \\ 0 \end{pmatrix} > \tag{98}$$

and, hence, in (97):

$$\langle \mathbf{f}_{k_1}^{(+)} | q(\epsilon x) | \mathbf{f}_{k_2} \rangle = \tilde{q}\left(\frac{k_1 - k_2}{\epsilon} \right) - \left\langle \mathbf{f}_{k_1}^{(+)} \middle| e^{ik_2 x} \{ 2iq'(\epsilon x)[k_2 + i\,\tanh(x)] + q''(\epsilon x) \} \middle| \begin{pmatrix} 1 \\ 0 \end{pmatrix} \right\rangle \tag{99}$$

where the bar denotes the derivative with respect to x. Similarly, we obtain for

$$\langle \overline{\mathbf{f}}_{k_1}^{(+)} | q(\epsilon x) | \mathbf{f}_{k_2} \rangle = -\left\langle \overline{\mathbf{f}}_{k_1}^{(+)} \middle| e^{ik_2 x} \{ 2iq'(\epsilon x)[k_2 + i\,\tanh(x)] + q''(\epsilon x) \} \middle| \begin{pmatrix} 1 \\ 0 \end{pmatrix} \right\rangle \tag{100}$$

and

$$\langle \mathbf{f}_{w,\theta,p,t}^{(+)} | q(\epsilon x) | \mathbf{f}_{k_2} \rangle = \left\langle \mathbf{f}_{w,\theta,p,t}^{(+)} \middle| e^{ik_2 x} \{ 2iq'(\epsilon x)[k_2 + i\,\tanh(x)] + q''(\epsilon x) \} \middle| \begin{pmatrix} 1 \\ 0 \end{pmatrix} \right\rangle. \tag{101}$$

Thus, if the absorber response is slow, $\epsilon \ll 1$, the derivatives are of the order

$$\begin{aligned} q'(\epsilon x) &= O(\epsilon) \\ q''(\epsilon x) &= O(\epsilon^2). \end{aligned} \tag{102}$$

In this case, we can safely neglect the higher order terms in (99) and (100) and we obtain only the diagonal coupling of the continuum modes and no coupling between soliton and the continuum. However, this is not truly the case for the absorber considered in (3), because we obtain

$$q'(\epsilon x) = -\epsilon(q - q_0) - \frac{W_0}{2E_A}\, q\,\mathrm{sech}^2(x). \tag{103}$$

Thus, only the term due to the absorber recovery scales properly with time. The saturation due to the soliton happens of course on the time scale of the soliton. However, with (103) this term is proportional to the overlap of the soliton with the nonsaturated absorber. This term never becomes larger than q_0, even if the absorber is strongly saturated. Therefore, it is legitimate to neglect this term in comparison with the δ-function like diagonal term. In total this shows, that a slow absorber leads to first order only to a diagonal coupling between the continuum modes and no coupling between the soliton and the continuum. Similar relations have been derived for the matrix elements of the gain dispersion operator in the appendix of [38].

Appendix B
Eigenvalues for the Complex Exponential Potential

Here, we give an analytic derivation of the eigenvalues for a Schrödinger equation with the complex exponential potential according to (81):

$$\left[-\overline{D}\, \frac{\partial^2}{\partial t^2} + V(t)(1 + i\alpha) \right] H_n(t) = -\tilde{\lambda}_n H_n(t) \tag{104}$$

with

$$V(t) = -V_0 \exp\left[-\frac{t}{\tau_A} \right], \quad \text{for } t > 0 \text{ and } v_s(t) = 0, \text{ elsewhere.} \tag{105}$$

We transform (104) into Bessel's differential equation by substitution of

$$y = 2\tau_A \sqrt{\frac{V_0(1 + i\alpha)}{\overline{D}}}\, \exp\left[-\frac{t}{2\tau_A} \right]. \tag{106}$$

Thus we obtain

$$\left[\frac{d^2}{dy^2} + \frac{1}{y}\, \frac{d}{dy} + \left(1 - \frac{\nu^2}{y^2} \right) \right] H_n(y) = \tilde{\lambda}_n H_n(y) \tag{107}$$

with

$$\nu = \sqrt{\frac{-2\tilde{\lambda}_n}{\overline{D}}}\, \tau_A \tag{108}$$

for $t > 0$. The solution of (107) is then given by

$$H_n(y) = AJ_\nu(y) + BY_\nu(y). \tag{109}$$

We require that the solution should stay bounded for $y \to 0$, i.e., $t \to \infty$, thus the constant B has to vanish. In the negative half space, where the potential vanishes, the solution is in general an exponential function. Matching of the two

solutions and their derivatives at $t = 0$ results in the following eigenvalue condition

$$J_{\nu-1}(z) = 0$$

with

$$z = \sqrt{\frac{V_0(1+i\alpha)}{\overline{D}}}\, 2\tau_A = 2\sqrt{\frac{1+i\alpha}{\frac{1}{D_n}+i}}\, w_A \tag{110}$$

where w_A is the normalized absorber recovery time according to (88). If the laser parameters are fixed, the complex argument z of the Bessel function is fixed and we have to find those complex orders ν, where the Bessel function vanishes. Since these values are easily computed for real arguments, we find it for complex arguments, i.e., $\alpha, D \neq 0$, by analytic continuation into the complex plane. We used a homotopy method that follows the trajectory of the complex roots when increasing the values of α, D from zero to their nominal values, (Fig. 10).

ACKNOWLEDGMENT

The authors acknowledge the careful reading of the manuscript by N. Matuschek, and many helpful discussions with Dr. U. Siegner concerning the carrier dynamics in semiconductors.

REFERENCES

[1] J. A. Valdmanis and R. L. Fork, "Design considerations for a femtosecond pulse laser balancing self phase modulation, group velocity dispersion, saturable absorption, and saturable gain," *IEEE J. Quantum Electron.*, vol. 22, pp. 112–118, 1986.
[2] D. E. Spence, P. N. Kean, and W. Sibbett, "60-fsec pulse generation from a self-mode-locked Ti:Sapphire laser," *Opt. Lett.*, vol. 16, pp. 42–44, 1991.
[3] D. K. Negus, L. Spinelli, N. Goldblatt, and G. Feugnet, "Sub-100 femtosecond pulse generation by Kerr lens modelocking in Ti:Sapphire," in *Advanced Solid-State Lasers*, G. Dube and L. Chase, Eds. Washington, DC: Opt. Soc. Amer., 1991, vol. 10, pp. 120–124.
[4] U. Keller, G. W. 'tHooft, W. H. Knox, and J. E. Cunningham, "Femtosecond pulses from a continuously self-starting passively mode-locked Ti:Sapphire laser," *Opt. Lett.*, vol. 16, pp. 1022–1024, 1991.
[5] C. Spielmann, P. F. Curley, T. Brabec, and F. Krausz, "Ultrabroadband femtosecond lasers," *IEEE J. Quantum Electron.*, vol. 30, pp. 1100–1114, 1994.
[6] J. Zhou, G. Taft, C.-P. Huang, M. M. Murnane, H. C. Kapteyn, and I. P. Christov, "Pulse evolution in a broad-bandwidth Ti:sapphire laser," *Opt. Lett.*, vol. 19, pp. 1149–1151, 1994.
[7] A. Stingl, M. Lenzner, C. Spielmann, F. Krausz, and R. Szipöcs, "Sub-10-fs mirror-controlled Ti:sapphire laser," *Opt. Lett.*, vol. 20, pp. 602–604, 1995.
[8] L. Xu, C. Spielmann, F. Krausz, and R. Szipöcs, "Ultrabroadband ring oscillator for sub-10 fs pulse generation," *Opt. Lett.*, vol. 21, pp. 1259–1261, 1996.
[9] T. Brabec, C. Spielmann, and F. Krausz, "Limits of pulse shortening in solitary lasers," *Opt. Lett.*, vol. 17, pp. 748–750, 1992.
[10] R. Szipöcs, K. Ferencz, C. Spielmann, and F. Krausz, "Chirped multilayer coatings for broadband dispersion control in femtosecond lasers," *Opt. Lett.*, vol. 19, pp. 201–203, 1994.
[11] M. Piche and F. Salin, "Self-mode locking of solid-state lasers without apertures," *Opt. Lett.*, vol. 18, pp. 1041–1043, 1993.
[12] T. Brabec, C. Spielmann, P. F. Curley, and F. Krausz, "Kerr lens modelocking," *Opt. Lett.*, vol. 17, pp. 1292–1294, 1992.
[13] I. P. Christov, H. C. Kapteyn, M. M. Murnane, C. P. Huang, and J. Zhou, "Space-time focusing of femtosecond pulses in a Ti:sapphire laser," *Opt. Lett.*, vol. 20, pp. 309–311, 1995.
[14] G. Cerullo, S. De Silvestri, V. Magni, and L. Pallaro, "Resonators for Kerr-lens mode-locked femtosecond Ti:sapphire lasers," *Opt. Lett.*, vol. 19, pp. 807–809, 1994.
[15] G. Cerullo, S. De Silvestri, and V. Magni, "Self-starting Kerr lens mode-locking of a Ti:sapphire laser," *Opt. Lett.*, vol. 19, pp. 1040–1042, 1994.
[16] A. Kasper and K. J. Witte, "10-fs pulse generation from a unidirectional Kerr-lens mode-locked Ti:sapphire laser," *Opt. Lett.*, vol. 21, pp. 360–362, 1996.
[17] S. T. Cundiff, W. H. Knox, E. P. Ippen, and H. A. Haus, "Frequency-dependent mode size in broadband Kerr-lens mode locking," *Opt. Lett.*, vol. 21, pp. 662–664, 1996.
[18] F. X. Kärtner, and U. Keller, "Stabilization of soliton-like pulses with a slow saturable absorber," *Opt. Lett.*, vol. 20, pp. 16–18, 1995.
[19] O. E. Martinez, R. L. Fork, and J. P. Gordon, "Theory of passively mode-locked lasers for the case of a nonlinear complex propagation coefficient," *J. Opt. Soc. Amer. B*, vol. 2, pp. 753–760, 1985.
[20] H. A. Haus, J. G. Fujimoto, and E. P. Ippen, "Structures for additive pulse modelocking," *J. Opt. Soc. Amer. B*, vol. 8, pp. 2068–2076, 1991.
[21] A. Hasegawa and Y. Kodama, "Guiding-center soliton," *Phys. Rev. Lett.*, vol. 66, pp. 161–164, 1991.
[22] V. E. Zakharov and A. B. Shabat, "Exact theory of two-dimensional self-focusing and one-dimensional self-modulation of waves in nonlinear media," *Zh. Eksp. Teor. Fiz.*, vol. 34, pp. 61–68, 1971; *Sov. Phys.-JETP*, vol. 34, pp. 62–69, 1972.
[23] S. M. J. Kelly, "Characteristic sideband instability of periodically amplified average solitons," *Electron. Lett.*, vol. 28, pp. 806–807, 1992.
[24] J. N. Elgin and S. M. J. Kelly, "Spectral modulation and the growth of resonant modes associated with periodically amplified solitons," *Opt. Lett.*, vol. 21, pp. 787–789, 1993.
[25] E. P. Ippen, "Principles of passive mode locking," *Appl. Phys.*, vol. B 58, pp. 159–170, 1994.
[26] H. A. Haus, J. G. Fujimoto, and E. P. Ippen, "Analytic theory of additive pulse and Kerr lens mode locking," *IEEE J. Quantum Electron.*, vol. 28, pp. 2086–2095, 1995.
[27] G. H. C. New, "Pulse evolution in mode-locked quasicontinuous lasers," *IEEE J. Quantum Electron.*, vol. 10, pp. 115–124, 1974.
[28] H. A. Haus, "Theory of mode locking with a slow saturable absorber," *IEEE J. Quantum Electron.*, vol. 11, pp. 736–746, 1975.
[29] I. D. Jung, F. X. Kärtner, L. R. Brovelli, M. Kamp, and U. Keller, "Experimental verification of soliton modelocking using only a slow saturable absorber," *Opt. Lett.*, vol. 20, pp. 1892–1894, 1995.
[30] R. Fluck, I. D. Jung, F. X. Kärtner, G. Zhang, F. X. Kärtner, and U. Keller, "Broadband saturable absorber for 10 fs pulse generation," *Opt. Lett.*, vol. 21, pp. 743–745, 1996.
[31] H. A. Haus, "Theory of modelocking with a fast saturable absorber," *J. Appl. Phys.*, vol. 46, p. 3049, 1975.
[32] H. Haken, *Advanced Synergetics.* Berlin: Springer Verlag, 1983.
[33] H. Haug and S. W. Koch, *Quantum Theory of the Optical and Electronic Properties of Semiconductors.* Singapore: World Scientific, 1986, p. 301.
[34] H. T. Moon, P. Huerre, and L. G. Redekopp, "Three-frequency motion and chaos in the Ginzburg–Landau equation," *Phys. Rev. Lett.*, vol. 49, pp. 458–460, 1982.
[35] K. Nozaki and N. Bekki, "Pattern selection and spatiotemporal transition to chaos in the Ginzburg–Landau equation," *Phys. Rev. Lett.*, vol. 51, pp. 2171–2174, 1983.
[36] J. P. Gordon, "Dispersive perturbations of solitons of the nonlinear Schrödinger equation," *J. Opt. Soc. Amer. B*, vol. 9, pp. 91–97, 1992.
[37] Y. S. Kivshar and B. A. Malomed, "Dynamics of solitons in nearly integrable systems," *Rev. Mod. Phys.*, vol. 61, pp. 763–915, 1989.
[38] F. X. Kärtner, D. Kopf, and U. Keller, "Solitary pulse stabilization and shortening in actively mode-locked lasers," *J. Opt. Soc. Amer. B*, vol. 12, pp. 426–438, 1995.
[39] G. P. Agrawal, *Nonlinear Fiber Optics.* New York: Academic, 1989.
[40] R. W. Schönlein, W. Z. Lin, E. P. Ippen, and J. G. Fujimoto, "Femtosecond hot-carrier energy relaxation in GaAs," *Appl. Phys. Lett.*, vol. 51, pp. 2134–2141, 1987.
[41] P. C. Becker, H. L. Fragnito, C. H. B. Cruz, R. L. Fork, J. E. Cunningham, and C. V. Shank, "Femtosecond photon echoes from band-to-band transitions in GaAs," *Phys. Rev. Lett.*, vol. 61, pp. 1647–1649, 1988.
[42] F. M. Mitschke and L. F. Mollenauer, "Discovery of the soliton self-frequency shift," *Opt. Lett.*, vol. 11, pp. 659–661, 1986.
[43] J. P. Gordon, "Theory of the soliton self-frequency shift," *Opt. Lett.*, vol. 11, pp. 662–664, 1986.

[44] U. Keller, F. X. Kärtner, D. Kopf, B. Braun, I. D. Jung, R. Fluck, C. Hönninger, and J. A. d. Au, this issue, pp. 435–543.
[45] W. H. Knox, D. S. Chemla, G. Livescu, J. E. Cunningham, and J. E. Henry, "Femtosecond carrier thermalization in dense fermi seas," *Phys. Rev. Lett.*, vol. 61, pp. 1290–1293, 1988.
[46] Y. H. Lee, A. Chavez-Pirson, S. W. Koch, H. M. Gibbs, S. H. Park, J. Morhange, N. Peyghambarian, L. Banyai, A. C. Gossard, and W. Wiegmann, "Room-temperature optical nonlinearities in GaAs," *Phys. Rev. Lett.*, vol. 57, pp. 246–249, 1986.
[47] L. Banyai and S. W. Koch, "A simple theory for the effects of plasma screening on the optical spectra of highly excited semiconductors," *Z. Phys.*, vol. 63, p. 283, 1986.
[48] J. P. Löwenau, F. M. Reich, and E. Gornik, "Many-body theory of room-temperature optical nonlinearities in bulk semiconductors," *Phys. Rev. B*, vol. 51, pp. 4159–4165, 1995.
[49] S. Flügge, *Practical Quantum Mechanics.* Berlin, Germany: Springer Verlag, 1934.
[50] H. A. Haus, "Parameter ranges for CW passive modelocking," *IEEE J. Quantum Electron.*, vol. QE-12, pp. 169–176, 1976.
[51] F. X. Kärtner, L. R. Brovelli, D. Kopf, M. Kamp, I. Calasso, and U. Keller, "Control of solid-state laser dynamics by semiconductor devices," *Opt. Eng.*, vol. 34, pp. 2024–2036, 1995.

F. X. Kärtner, for photograph and biography, see this issue, p. 452.

I. D. Jung, for photograph and biography, see this issue, p. 452.

U. Keller, for photograph and biography, see this issue, p. 452.